Global Change Biology

Global Change Biology (2016) **22**, 3414–3426, doi: 10.1111/gcb.13258

Global vegetation productivity response to climatic oscillations during the satellite era

ALEMU GONSAMO[1], JING M. CHEN[1] and DANICA LOMBARDOZZI[2]

[1]*Department of Geography and Planning, University of Toronto, Toronto, ON, Canada, M5S 3G3,* [2]*National Center for Atmospheric Research, P.O. Box 3000, Boulder, CO 80307, USA*

Abstract

Climate control on global vegetation productivity patterns has intensified in response to recent global warming. Yet, the contributions of the leading internal climatic variations to global vegetation productivity are poorly understood. Here, we use 30 years of global satellite observations to study climatic variations controls on continental and global vegetation productivity patterns. El Niño-Southern Oscillation (ENSO) phases (La Niña, neutral, and El Niño years) appear to be a weaker control on global-scale vegetation productivity than previously thought, although continental-scale responses are substantial. There is also clear evidence that other non-ENSO climatic variations have a strong control on spatial patterns of vegetation productivity mainly through their influence on temperature. Among the eight leading internal climatic variations, the East Atlantic/West Russia Pattern extensively controls the ensuing year vegetation productivity of the most productive tropical and temperate forest ecosystems of the Earth's vegetated surface through directionally consistent influence on vegetation greenness. The Community Climate System Model (CCSM4) simulations do not capture the observed patterns of vegetation productivity responses to internal climatic variations. Our analyses show the ubiquitous control of climatic variations on vegetation productivity and can further guide CCSM and other Earth system models developments to represent vegetation response patterns to unforced variability. Several winter time internal climatic variation indices show strong potentials on predicting growing season vegetation productivity two to six seasons ahead which enables national governments and farmers forecast crop yield to ensure supplies of affordable food, famine early warning, and plan management options to minimize yield losses ahead of time.

Keywords: climatic oscillation, community climate system model, crop yield forecasting, El Niño-Southern Oscillation, normalized difference vegetation index, precipitation, radiation, remote sensing, teleconnection, temperature

Received 9 October 2015 and accepted 14 February 2016

Introduction

The global ocean-atmosphere system has several internal patterns of variability, which modulate the location and strength of storm tracks and fluxes of heat, moisture and momentum. While a few patterns appear to be primarily atmospheric in origin (for example, the North Atlantic Oscillation NAO), many are connected to anomalous sea surface temperature (SST) patterns that systematically change the precipitation and heating patterns (such as El Niño-Southern Oscillation ENSO), and generate teleconnections downstream (Wallace & Gutzler, 1981; Barnston & Livezey, 1987; Lau & Nath, 1994; Sheng, 1999; Trenberth & Smith, 2005; Hurrell & Deser, 2010). Accordingly, some regions are more anticyclonic than normal and provide persistent sunny and drier conditions, while other regions are more cyclonic, with more storms, rain, cloud and soil moisture. In between storm tracks are altered. The resulting spatial teleconnections are expressed using teleconnection indices relating oceanic and atmospheric climate anomalies at large distances (Barnston & Livezey, 1987; Trenberth & Smith, 2005).

Understanding the nature and variations in the behaviours of teleconnection patterns is central to understanding seasonal predictability of regional vegetation productivity and crop yield (Garnett *et al.*, 1998; Hsieh *et al.*, 1999; Quiring & Blair, 1999; Iizumi *et al.*, 2014; Gonsamo & Chen, 2015), and their links to rainfall, snowfall, droughts, temperature and cloud cover and associated incident solar radiation patterns. Prominent teleconnection patters such as ENSO show that El Niño years are related on land with reduced precipitation (that instead occurs over the high SSTs over the ocean), continental freshwater discharge (Dai *et al.*, 2009) and evapotranspiration (Miralles *et al.*, 2013) over many land areas, while wetter land occurs during La Niña years (Trenberth *et al.*, 2014a). Hence, the internal climatic variability (hereafter referred to as 'climatic variability' as opposed to externally forced 'climate change'), such as ENSO, also affects the interpretation

Correspondence: Alemu Gonsamo, tel. +1 416 946 7715, fax +1 416 946 3886, e-mail: gonsamoa@geog.utoronto.ca

of the historic Palmer Drought Severity Index (Trenberth *et al*., 2014a) trends and relations to climate change. Evidently El Niño years promote more droughts and limited terrestrial moisture supply resulting in enhanced plant moisture stress through greater moisture demand along with the concomitant increase in continental temperature. Therefore, teleconnection patterns are strong indicators of the regional and global carbon budgets of the terrestrial biosphere and of total plant photosynthesis.

The total amount of carbon gained by the terrestrial biosphere is partly regulated by climatic variability, and therefore responds to a wide range of teleconnection patterns. Terrestrial carbon gain is manifested in the light-harvesting capacity of plants, which can be monitored remotely by changes in the Normalized Difference Vegetation Index (NDVI). Although, NDVI is not an intrinsic physical productivity measure, the growing season integrated NDVI value is widely used as a surrogate of primary productivity of the terrestrial biosphere (Myneni *et al*., 1997), and indicates the rate of organic biomass growth and accumulation by plants. Several teleconnection indices are linked to regional NDVI variability (Gong & Shi, 2003; Woodward *et al*., 2008). Well-studied ENSO dynamics show that during warm ENSO (El Niño) events, the global terrestrial biosphere decreases both in net and total productivity, whereas during cool ENSO (La Niña) events, the terrestrial carbon sink capacity increases (Patra *et al*., 2005; Miralles *et al*., 2013). However, no clear global-scale vegetation productivity response related to ENSO phases has been reported (Behrenfeld *et al*., 2001), and no studies have determined global vegetation responses to other leading teleconnection patterns. Such limited information makes the overall impacts of internal climatic variations on global-scale terrestrial primary productivity uncertain, and further hinders crop yield predictability and regional climate forecasting ability, important for determining agricultural regions under future climate scenarios. With accumulation of satellite observations over the last three decades, we can now study the roles of teleconnection patterns on long-term trends and interannual variability of global and regional vegetation productivity.

Here, we use 30 years (1982–2011) of bi-monthly 8 km satellite $NDVI_{3g}$ data, annual growing season values, from the Global Inventory Modelling and Mapping Studies (GIMMS) (Pinzon & Tucker, 2014) to show the impacts of eight leading teleconnection patterns on global vegetation productivity. Data for the eight teleconnection indices (Wallace & Gutzler, 1981; Barnston & Livezey, 1987), namely the NAO, East Atlantic Pattern (EA), West Pacific Pattern (WP), Pacific/ North American Pattern (PNA), East Atlantic/West Russia Pattern (WR), Scandinavia Pattern (SCA), Polar/ Eurasia Pattern (POL) and ENSO-Niño 3.4 index (NINO), were obtained from the National Oceanic and Atmospheric Administration (NOAA) National Weather Service. We also use the gridded Climatic Research Unit (CRU TS 3.21) (Harris *et al*., 2014) annual growing season mean temperature and total precipitation data at 0.5×0.5 degree, and the Clouds and Earth's Radiant Energy System (CERES) downwelling total shortwave surface radiation data downscaled from 1×1 to 0.5×0.5 degrees to investigate the biophysical mechanisms of teleconnection controls on the interannual variability of global vegetation productivity.

Our goal is to determine how much teleconnection indices control the spatial pattern of global vegetation productivity through mediation of meteorological variables. Therefore, our objectives are: (i) to study the long-term trend of NDVI in relation to decadal and multidecadal teleconnection indices; (ii) to study the interannual relationship between vegetation productivity and teleconnection indices those with intraannual and interannual frequencies of variability; and (iii) to evaluate the winter time teleconnection indices for crop yield forecasting ability with a few months lead time. We use satellite observed NDVI and modelled net primary productivity (NPP) as proxies of vegetation productivity. We do not imply that NDVI from satellite sensor is equivalent to NPP both are independent but related measures of vegetation productivity. Our aim is not to explain the entire interannual and long-term variances in vegetation productivity. Therefore, other nonclimatic causes on vegetation productivity patterns are discussed only if they coincide in the direction of influence with teleconnection phases.

Materials and methods

Data

Satellite NDVI data. The 30-year (1982–2011) measurements of Normalized Difference Vegetation Index (NDVI) are obtained from the bi-monthly 8 km Global Inventory Modelling and Mapping Studies (GIMMS) third-generation ($NDVI_{3g}$) (Pinzon & Tucker, 2014) observations that are derived from satellite-based surface reflectance aboard the Advanced Very High Resolution Radiometer (AVHRR) series of sensors. NDVI is defined as the ratio of the difference between near-infrared reflectance and red visible reflectance to their sum. NDVI values <0.1 (Defries & Townshend, 1994; Markon *et al*., 1995; Hird & Mcdermid, 2009) were removed from the entire analysis, as they were interpreted to be from the nongrowing season and nonvegetated land pixels.

Climate data. The annual growing season mean temperature and total precipitation data were obtained from the monthly

gridded Climatic Research Unit (CRU TS 3.21) (Harris *et al*., 2014) data at 0.5 × 0.5 degree resolutions for 1981–2011. The annual growing season total all sky downwelling shortwave surface radiation data at 1.0 × 1.0 degree resolutions for 2001–2011 was obtained from the National Aeronautics and Space Administration (NASA) Clouds and Earth's Radiant Energy System (CERES) Energy Balanced and Filled (EBAF) monthly product (http://ceres-tool.larc.nasa.gov). The CERES EBAF downwelling shortwave radiation (version CERES_EBAF-Surface_Ed2.8_S) is the computed downward shortwave flux based on the Langley Fu-Liou radiative transfer model (Fu & Liou, 1992, 1993; Fu, 1996; Fu *et al*., 1998). Details of CERES EBAF-surface product description and methodology are given in (Kato *et al*., 2013). The radiation data used in this study were retrieved on March 08, 2015. Product updates are given in Ed2.8 Data Quality Summary (http://ceres.larc.nasa.gov/products.php?product=EBAF-Surface).

Teleconnection index data. We restricted the teleconnection indices to those that dominate the interannual variability of climatic variations in phase and amplitude with continental to global-scale implications accounting for the most spatial variance of the observed standardized anomaly (Quadrelli & Wallace, 2004; IPCC, 2007). The eight teleconnection indices: North Atlantic Oscillation (NAO), East Atlantic Pattern (EA), West Pacific Pattern (WP), Pacific/ North American Pattern (PNA), East Atlantic/West Russia Pattern (WR), Scandinavia Pattern (SCA), Polar/ Eurasia Pattern (POL) and ENSO-Niño 3.4 index (NINO), were obtained from the National Oceanic and Atmospheric Administration (NOAA) National Weather Service website (www.cpc.ncep.noaa.gov). The procedure used to calculate the teleconnection indices except NINO, is based on the Rotated Principal Component Analysis (RPCA) applied to monthly mean standardized 500-mb height anomalies (Barnston & Livezey, 1987) in the analysis region 20°N–90°N by isolating the primary teleconnection patterns for all months and allowing time series of the patterns to be constructed. The RPCA procedure is superior to grid-point-based analyses, typically determined from one-point correlation maps, in that the teleconnection patterns in the RPCA approach are identified based on the entire flow field, and not just from height anomalies at select locations. The standardized monthly anomaly fields are determined in the three-month period centred on that month. NINO is calculated from monthly Niño-3.4 index that uses 1981–2010 base period to calculate departures (http://www.cpc.ncep.noaa.gov/products/analysis_monitoring/ensostuff/detrend.nino34.ascii.txt).

We calculated teleconnection index anomalies for each year as a mean value of December of the preceding year and January, February and March of the current year. We then removed trends from the resulting winter teleconnection index by detrending the time series for 1981–2011 base period, encompassing the time frame of the climate and NDVI data used in this study. The El Niño years were defined as five consecutive overlapping 3-month periods, at or above, the +1.5 NINO index anomaly, La Niña years at or below the −1.5 anomaly, and neutral years between −0.5 and +0.5 anomaly. ENSO phase year is a year starting from July of the preceding year to June of the current year. El Niño event years were, 1983, 1988 and 1998. La Niña event years were, 1989, 2000 and 2011. Neutral ENSO event years were, 1982, 1990, 1991, 1993, 1994, 1997 and 2002.

In order to identify the long-term trend relationship between NDVI and decadal climatic variations, we obtained the Pacific Decadal Oscillation (PDO) (http://www.ncdc.noaa.gov/teleconnections/pdo/) and Atlantic Multidecadal Oscillation (AMO) (http://www.esrl.noaa.gov/psd/data/timeseries/AMO/) from NOAA. The temporally smoothed PDO data were interpreted negative phase for 1999–2011 and positive PDO phase for 1982 1998 (Trenberth *et al*., 2014b), while the AMO interpreted positive for 1995–2011 and negative AMO phase for 1982 1994. The NOAA's National Climatic Data Center (NCDC) PDO index is based on NOAA's Extended Reconstructed Sea Surface Temperature (ERSST version 3) (Smith *et al*., 2008). The AMO is calculated from the Kaplan SST dataset (Kaplan *et al*., 1998).

Modelling. Net primary productivity (NPP) was simulated using the Community Climate System Model version 4 (CCSM4) which consists a finite volume nominal 1° (0.9° × 1.25°) 26-level implementation of the Community Atmosphere Model version 4 (CAM4) with coupled ocean, land and sea ice components. The land component, the Community Land Model version 4 (CLM4), includes a terrestrial carbon cycle. A seven-member ensemble of CCSM4 simulations with different initialization and using historic forcing were analysed for 1982–2005 (Lombardozzi *et al*., 2014). The resulting annual ensemble mean NPP, temperature and precipitation, and the standard deviation of the seven-member ensemble gridded NPP values were acquired, and detrended to remove the long-term trends. We represent NPP standard deviation (noise) as unforced values due to internal climatic variability and mean (signal) as forced values.

Analyses

The NDVI data were averaged to monthly values from the bi-weekly time scale. Then NDVI values below 0.1 were removed from the entire analysis, as they were interpreted to be from the nongrowing season and nonvegetated land pixels. Those areas which did not have data for the entire 30 years of study period were also removed from analyses. The annual sum NDVI values were obtained for the growing season only at native 8 × 8 km spatial resolution. These data were used to study the NDVI trend and relationships to PDO and AMO and NDVI responses to long-term variabilities in annual growing season temperature and precipitation (Fig. S1). In the remaining analyses, the trends were removed at annual time scale to study the interannual relationship between NDVI and teleconnection patterns at native 8 × 8 km spatial resolution (Fig. 3). We have done further sensitivity analysis on impacts of eight leading teleconnection patterns on global annual growing season NDVI anomaly during teleconnection phase years at 8 × 8 km native NDVI, 0.5 × 0.5 degree native CRU climate data, and 1.25 × 0.9 degree native CCSM4 NPP spatial resolutions

(Fig. S2). The results show that different spatial resolutions do not affect the teleconnection pattern relations to growing season NDVI values. The monthly solar radiation data were also bilinearly interpolated to 0.5 × 0.5 degree from its native 1 × 1 degree spatial resolution. The monthly NDVI and climatic data were integrated to annual time scales using the growing season months only after removing, NDVI values below 0.1, those grids which did not have growing season NDVI values for the entire 30 years, and interpolating to common 0.5 × 0.5 degree spatial resolution. The new annual growing season datasets were deterended at annual time scale based on the common base period of each analysis using the entire available time series period, for example, for NDVI vs. teleconnection, the base period is 1982 2011 and for radiation vs. teleconnection, the base period is 2001 2011.

We use the winter, defined here as December of the preceding year and January, February and March of the NDVI year, teleconnection indices for the following two reasons: (i) most of the leading teleconnection indices are only active during the northern hemisphere winter, and (ii) they provide predictive power for summer time crop yield forecasting in northern hemisphere ahead of time (Gonsamo & Chen, 2015). In order to encompass the time period beyond the coincident calendar period, we also study the lagged impact of teleconnection patterns on the ensuing year NDVI, NPP and climate data values. A seven-member ensemble of CCSM4 simulations with different initialization were used to obtain annual ensemble mean (signal) and standard deviation (noise) NPP (Lombardozzi *et al*., 2014).

To increase the confidence in our findings and minimize the detection of spurious correlations, the interannual covariability analyses amongst NDVI, climate, and teleconnection indices were conducted only from detrended data. The original raw data were only used in Figs 1 and S1 to analyse the impacts of long-term trends of PDO, AMO, temperature and precipitation on NDVI. In order to remove the effect of temporal autocorrelation that may occur at monthly or seasonal time scales, we only use annual growing season NDVI (values >0.1), growing season total precipitation, total radiation and mean temperature, and winter period teleconnection indices. All significance levels reported in this study have been estimated with a two-tailed Student's *t*-test (95%-level).

To remove multicollinearity in multivariate analysis among several teleconnection indices, temperature, radiation and precipitation, we employ principal component analysis (PCA), also called empirical orthogonal function (EOF) analysis to produce eight new orthogonal independent teleconnection indices. There were strong correlations among several teleconnection indices (Table S1). Each of the original teleconnection indices contributed to the resulting variances in all eight PCAs (Table S2). For example, NINO explains most of the variances in PCA 7, whereas EA contributes the maximum to PCA 5. Therefore, we have not conducted the commonly applied stepwise regression to eliminate PCAs that contribute the least to the obtained variances. Finally, we used all eight PCAs to analyse the relationships of teleconnection indices to precipitation, radiation and temperature.

Results

This section starts with the results of long-term trends of the growing season NDVI in relation to decadal internal climatic variability followed by the interannual relationships between NDVI and high frequency teleconnection patterns. We then present the spatial distributions of each meteorological variable control on vegetation productivity and the roles of teleconnection patterns on regional meteorological variability to explain the interannual relationship between NDVI and teleconnection indices. We also present results from CCSM4 NPP simulations to test whether the observed relationships between teleconnection patterns and NDVI are captured by modelled productivity measures. Finally, given that the high frequency teleconnection indices used in this study are from the winter months, we apply the observed relationships between teleconnection indices and NDVI to predict summer time crop yield productivity using winter time teleconnection patterns.

Long-term trends of NDVI and climatic variability

The global growing season NDVI trend is mostly positive for the last 30 years, although negative trends are apparent in the Patagonian steppe, the boreal zones of Canada, the arid zones of the northern Sahel, the southern Sahara, the coastal lowlands of the horn of Africa, southern Arabia and the semiarid zones of Asia (Fig. 1a). Australia, Central Eurasia and Southern Africa are the three large regions equally controlled by both precipitation and temperature for long-term and interannual variabilities in vegetation productivity (Figs 1f,h and S1). The Patagonian steppe is highly correlated to precipitation (Figs 1f and S1); meaning that changes in precipitation and drought regimes may explain the declining trends in NDVI in this region (Figs 1 and S3). The positive trend in the global growing season NDVI largely follows the negative and positive years of Pacific Decadal Oscillation (PDO) and Atlantic Multidecadal Oscillation (AMO) (Fig. 1a–c).

Global and continental NDVI responses to ENSO

El Niño phase years have lesser impact on the continental vegetation productivity than neutral years, while La Niña phase years are the most important indicator of continental vegetation productivity (Figs 2a and S5) associated with cold and wet years of forested tropical areas (Fig. 4). A year after La Niña phase years, vegetation productivity increases throughout all regions of the world (Figs 2b and S5), as shown by NINO's globally well distributed negative correlations with ensuing

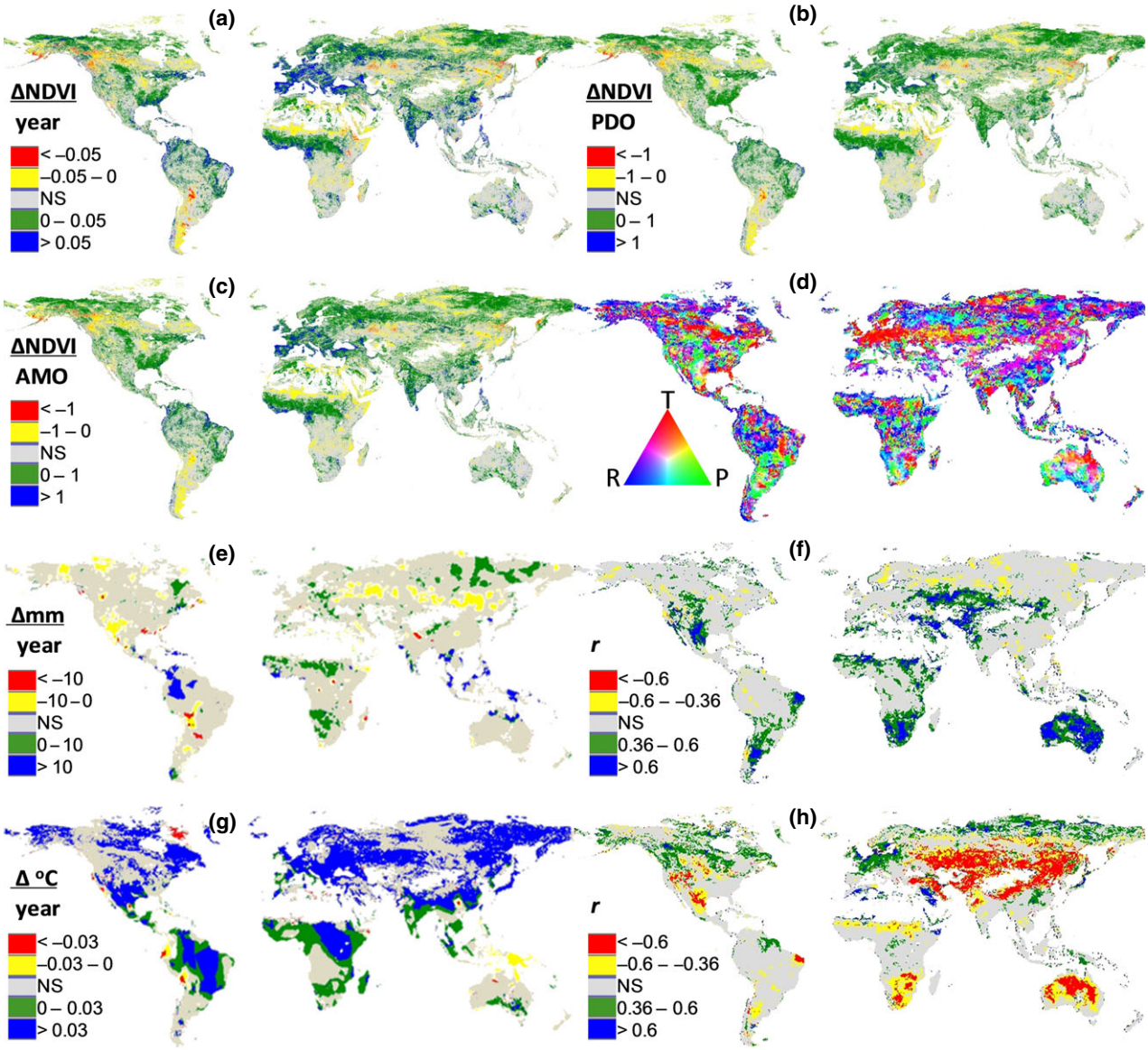

Fig. 1 Trends and interannual relationships among NDVI, precipitation, temperature and solar radiation. Trends in annual growing season NDVI sum (a), total precipitation (e) and mean temperature (g) for 1982–2011. Annual growing season NDVI sum difference between 1999 and 2011 negative PDO and 1982 1998 positive PDO (b) and 1995–2011 positive AMO and 1982 1994 negative AMO (c) for significant trends shown in (a). (d) Geographic distribution of temperature (T), precipitation (P) and solar radiation (R) controls on interannual vegetation productivity for 2001–2011. The climatic controls in (d) were calculated based on coefficient of determinations of NDVI against T, P and R for common measurement period 2001–2011. Values in (d) are normalized by dividing each channel value with the maximum coefficient of determination of each grid for clarity. Discrete map for (d) by assigning each grid channel only to its maximum meteorological variable control is given in Fig. S3 for further clarity. Growing season NDVI sum responses to interannual variabilities in precipitation (f) and temperature (h) for 1982–2011. All colour shaded values in (a, b, c, e, f, g, h) are significant at 95% confidence level from a two-tailed Student's *t*-test. *r* is Pearson correlation coefficient. NS is not statistically significant. (d, f, h) were calculated from detrended datasets at 0.5 × 0.5 degree. Trends in (a, b, c) were calculated from raw data at 8 × 8 km. The relationships among T, P and R are given in Fig. S4 for 2001–2011.

year NDVI (Fig. 3). The same is true during La Niña phase years, when vegetation productivity is increased except in North America and Oceania (Fig. 2a), mainly due to decreased moisture stress during the cold and wet La Niña years. Neutral phase years of ENSO are associated with decreased productivity of vegetation in South America and Australia, where the effect lasts to ensuing year NDVI (Fig. 2a,b).

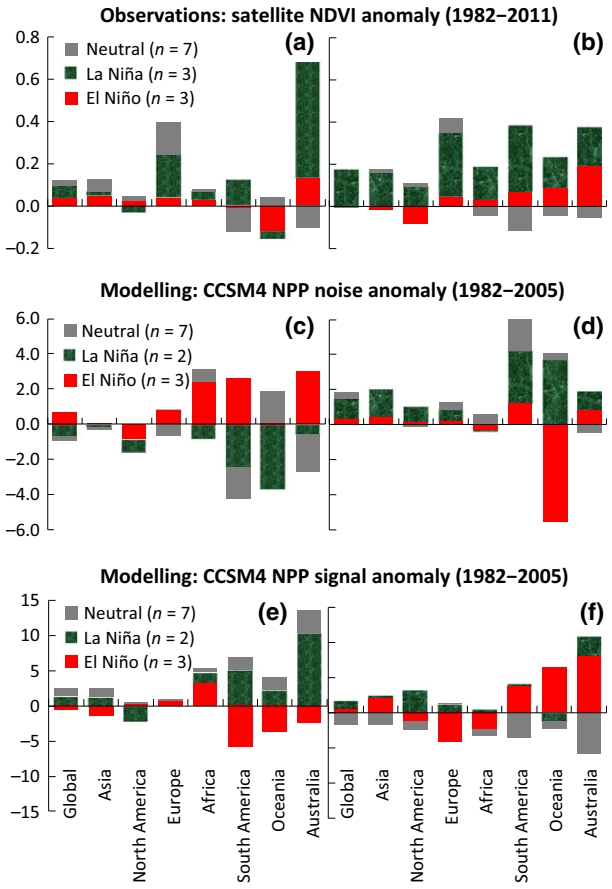

Fig. 2 Responses of NDVI and NPP anomalies to ENSO phases. Satellite measured global and continental mean annual growing season NDVI sum anomalies during (a) and one year after each phase of ENSO years (b). The Community Climate System Model version 4 (CCSM4) simulated standard deviation (noise) anomalies of the seven-member ensemble gridded NPP values representing the internal climatic variability during (c) and one year after each phase of ENSO years (d). The CCSM4 mean (signal) anomalies of the seven-member ensemble gridded NPP values (e) and one year after each phase of ENSO years (f). ENSO events are defined as five consecutive overlapping 3-month periods at, or above, the +1.5 NINO index anomaly for El Niño events, at or below the −1.5 anomaly for La Niña events, and between −0.5 and 0.5 for neutral events. ENSO phase year is a year starting from July of the preceding year to June of the current year. Both NDVI and NPP datasets were detrended.

Global and continental NDVI responses to other ENSO-like climatic variability

NAO is negatively correlated to vegetation productivity in the western hemisphere and positively correlated in central Europe, Southern Scandinavia, and midwestern Eurasia (Fig. 3) through its influence mainly on temperature (Fig. 4). Since the mid-1960s, there has been a positive trend towards higher NAO index values and concomitant winter warming in Europe and Asia (Hurrell & Deser, 2010). A steeper gradient (the high or positive NAO phase) that causes the westerly wind to pick up heat and carry it across central Europe and Asia, is associated with warmer Europe and Asia temperatures and colder and drier winters in Canada (Fig. 4). These asymmetric trends delay the spring greenup of the Canadian boreal vegetation and therefore productivity, and result in the opposite trend in Europe and Asia (Hurrell & Deser, 2010). We suspect that this partly explains the declining greenness in boreal Canada and increasing greenness in Europe and central Eurasia (Fig. 1a), as NAO was positive for 20 out of 30 years during the study period.

The SCA being negatively correlated with NAO (Table S1) is negatively correlated with vegetation productivity in central Europe and western Siberia (Fig. 3). The positive phase of the winter SCA causes cold-air accumulation over a vast area extending from western Europe to Siberia (Macias-Fauria *et al.*, 2012) (Fig. 4), and resulting in overall lower vegetation productivity in Europe (Fig. 3). Winter NAO and SCA can significantly ($P < 0.05$) explain vegetation productivity in most of central Europe, which makes them strong potential tools for crop yield prediction, particularly related to the recent and projected occurrences of heatwaves in this region (Trnka *et al.*, 2014) (Table 1).

Among the eight leading teleconnection patterns, the East Atlantic/West Russia Pattern (WR) is negatively correlated with the ensuing year NDVI values of the most productive forest ecosystems of the Earth's vegetated surfaces, such as the rain forests in Amazon- and Congo-basins and Southeast Asia, and the temperate and boreal forests in northeastern America (Fig. 3) through statistically weak impact on meteorological variables (Fig. 4) but directionally consistent influence on continental vegetation greenness (Gonsamo *et al.*, 2015) (Fig. S6). PNA is negatively correlated with NDVI of the ensuing year over North America, showing persistent lag effects on vegetation productivity (Fig. 3). PNA can explain the vegetation productivity of the ensuing year in most of the eastern United States, revealing a strong potential tool for crop yield prediction and drought monitoring in this region (Table 2). PNA is highly correlated with NINO (Table S1) and has a comparable effect on climate patterns as NINO during the phase and lagged years (Fig. 4), with eastward propagating SST anomalies in the North Pacific possibly related to the air-sea interactions in the North Pacific. The timescale for the SST anomalies to travel across the entire North Pacific is ~1 year (Sheng, 1999). Such wide spread and delayed impacts of PNA, WR, and NINO on vegetation productivity (Fig. 3) and meteorological variables (Fig. 4) provide further observational reinforcement of the oceanic and atmospheric bridge

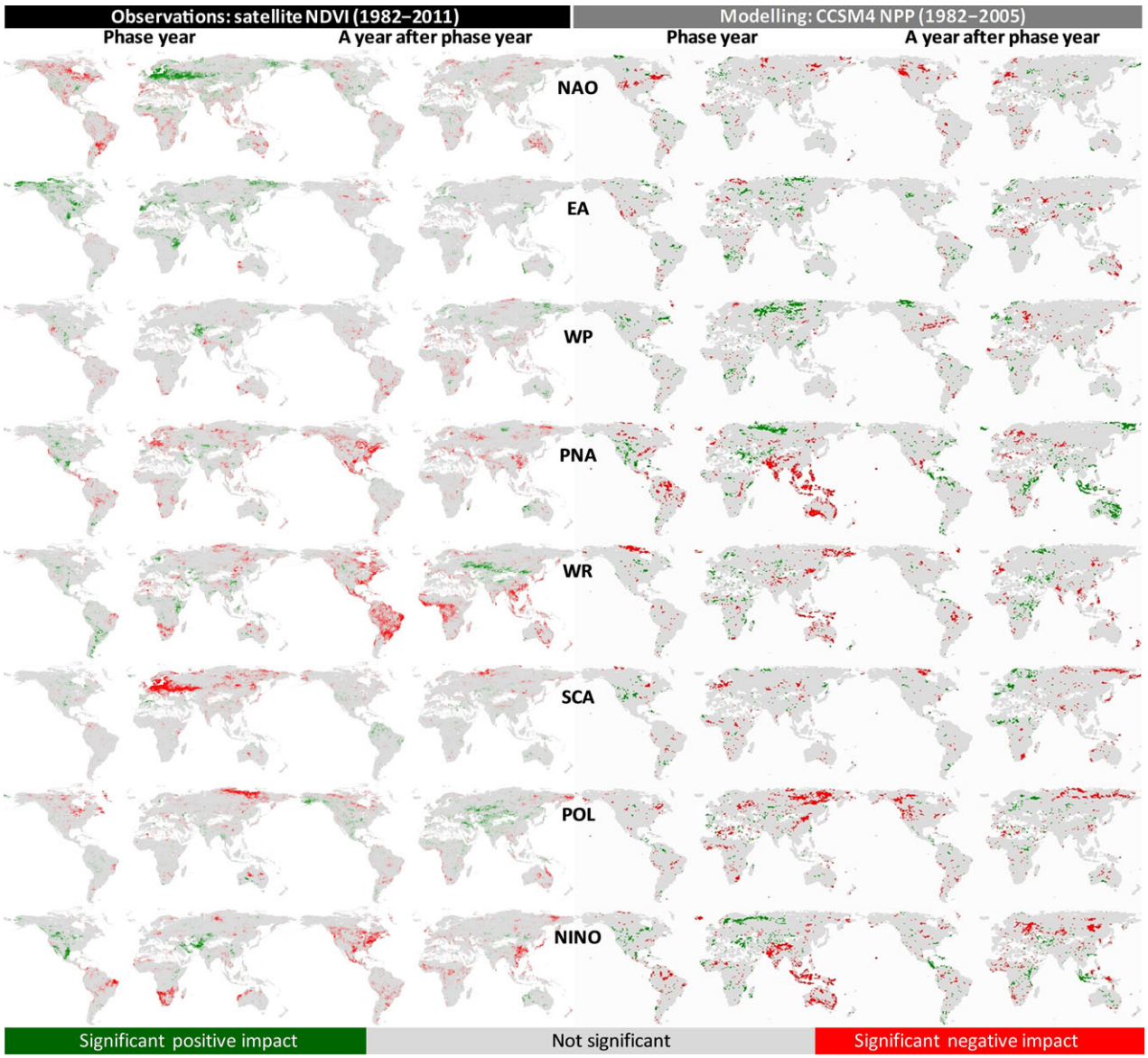

Fig. 3 Impacts of eight leading teleconnection patterns on global growing season NDVI and NPP anomalies during and the ensuing teleconnection phase years. The teleconnection anomalies are calculated as a mean value of December of the preceding year and January, February and March of the NDVI and NPP year. All teleconnection, NDVI and NPP datasets are detrended, and the modelled NPP is obtained from the Community Climate System Model version 4 simulated mean (signal) anomalies of the seven-member ensemble gridded NPP values. The relationships between teleconnection and standard deviation (noise) anomalies of the seven-member ensemble gridded NPP representing the internal climatic variability are given in Fig. S7. All colour shaded values are significant at 95% confidence level from a two-tailed Student's *t*-test.

theories(Lau & Nath, 1994) even at wider tropical-extratropical and interhemispheric geographic scales.

East Atlantic Pattern (EA), following the southeastward shifted nodal line of NAO, is positively correlated with the overall increases of vegetation productivity in most of the Earth's vegetated surfaces, with North America, southern Europe, and northwestern Siberia exhibiting the greatest responses (Fig. 3). WP is less capable of explaining the global distribution of vegetation productivity (Fig. 3) and the only index not significantly related with any of the remaining teleconnection indices (Table S1). POL, enhancing the strength of the circumpolar vortex during the positive phase, is negatively correlated with circumpolar vegetation productivity during the phase and ensuing years (Fig. 3) through its influence on temperature which extends from midwestern USA to North Africa and southwestern China (Fig. 4).

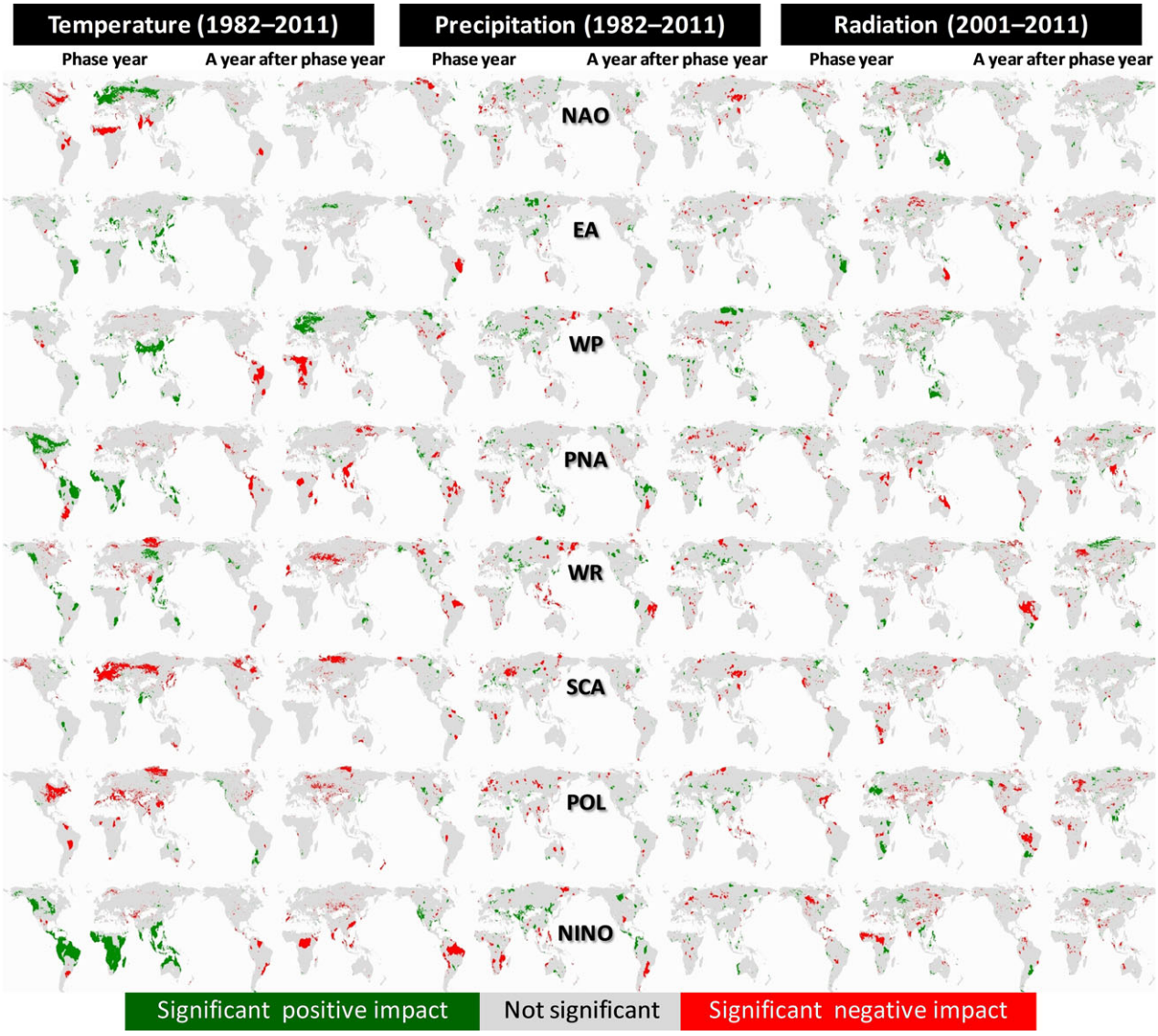

Fig. 4 Impacts of eight leading teleconnection patterns on global growing season temperature and precipitation for 1982–2011, and radiation for 2001–2011. Phase year is temperature, radiation and precipitation responses to teleconnection indices during the same year. A year after phase year is temperature, radiation and precipitation responses to teleconnection indices during the ensuing year. The teleconnection anomalies are calculated as a mean value of December of the preceding year and January, February and March of the temperature and precipitation year. All datasets were detrended. All colour shaded values are significant at 95% confidence level from a two-tailed Student's *t*-test.

Interannual changes of NDVI in response to meteorological variables

We have presented global distributions of temperature, precipitation and solar radiation controls on vegetation productivity for 2001–2011 (Figs 1d and S3). During the common measurement period 2001–2011, satellite and gridded climatic observations reveal that the interannual changes in global vegetation productivity are explained by temperature, radiation and precipitation over 33.2%, 34.3% and 32.5% of Earth's vegetated surface respectively (Fig. S3). Yet, the three meteorological variables co-explain interannual productivity for large portion of the Earth's surface (Fig. 1d). Prairie region in North America, Patagonia in South America, and parts of Australia's lowlands are highly controlled by precipitation (Figs 1d and S3). In pacific coastal temperate zones of North America, Amazon rainforest, and Eurasian high latitudes, radiation plays the highest role in explaining interannual changes in vegetation productivity.

Table 1 Predicting performances of eight leading teleconnection indices on country specific vegetation productivity for 1982–2011

Country	EA	NAO	NAO (lag)	NINO	PNA	PNA (lag)	SCA	SCA (lag)	WP	WR (lag)
Austria							–			
Belarus							–			
Cayman Islands						–				
Kenya	+									
Lao People's Democratic Republic										–
Liberia										–
Libya										
Liechtenstein							–			
Saint Martin			–							
Moldova							–			
Portugal	+									
Palestine				+						
Saint Helena			–							
Sierra Leone										–
Slovenia							–			
Seychelles			–							
Ukraine							–			
Belgium		+					–			
Czech Republic		+			–		–			
Germany		+					–			
Denmark		+			–		–			
Estonia		+					–			
Lithuania		+					–			
Luxembourg		+					–			
Latvia		+					–			
Netherlands		+					–			
Poland		+					–			
Saint Pierre and Miquelon		+								+

The teleconnection anomalies are calculated as a mean value of December of the preceding year and January, February and March of the NDVI year. Both teleconnection and NDVI datasets were detrended. + sign is for statistically significant positive and – sign is for statistically significant negative relationship between NDVI and the teleconnection indices at 95% confidence level from a two-tailed Student's *t*-test. (lag) is the predicting performances of teleconnection indices on the NDVI productivity of the ensuing year. Only countries where there is statistically significant predicting performance at 95% confidence level from a two-tailed Student's *t*-test are shown.

The Community Climate System Model simulation response to climatic variability

To test whether the observed global vegetation productivity responses to teleconnections were well represented in the current state-of-the-art Community Climate System Model version 4 (CCSM4), we examined a seven-member ensemble of CCSM4 simulations with different initialization (Lombardozzi *et al.*, 2014). All ensemble members were run with identical experimental conditions but with different initialization, each producing different climate trajectories which were assumed as climatic variability within the model arising from random internal variation. The modelled NPP is assumed as a surrogate value of the satellite measured NDVI (Myneni *et al.*, 1997), and standard deviations (noise) of the individual ensemble members are assumed to indicate the internal climatic variability partly represented by teleconnection indices. We found that, in contrast to the strong correlations between observed NDVI and teleconnections (Figs 2 and 3), the CCSM4 performed poorly in capturing the NPP correlations with teleconnection, even with the well-studied ENSO index (Figs 2 and S8). Neither the standard deviations (noise) NPP values show the observed teleconnection pattern control on vegetation productivity (Fig. S7). There are no significant relationships between global and continental mean NPP and NDVI (Fig. S8) while they are not equivalent we expected modest relationships for regional averaged values. The lack of relationships among the CCSM4 and teleconnection indices shows that CCSM4 simulations do not capture interannual covariability between NPP and meteorological variables.

Table 2 The same as Table 1 but for the USA states

US states	EA	NINO (lag)	PNA (lag)	WR (lag)
Wisconsin	+			
Maine			–	
Vermont			–	
Georgia			–	
District of Columbia		–		
West Virginia		–		
Maryland		–		
New York		–	–	
Pennsylvania		–	–	
Alabama				–
Mississippi				–
New Hampshire		–	–	–
Massachusetts		–	–	–
Connecticut		–	–	–
Rhode Island		–	–	–
New Jersey		–	–	–

Relationships among meteorological variables and climatic variability

Natural ocean-atmosphere variations interact to impose complex and varying limitations on climate (Fig. S9) and vegetation productivity (Figs 1d and S3) in various parts of the world. ENSO is highly correlated with EA, PNA and WR (Table S1) and contributes the highest to the obtained variance in the first PCA (Table S2). NAO, WR and SCA load the highest on the second PCA (Table S2) indicating these three indices are highly related to each other. In order to provide a comprehensive interpretation of interactions among ocean-atmosphere variations on global meteorological variables, we apply multivariate regression analysis on orthogonal variables of the eight teleconnection indices, transformed using principal component analysis (PCA) to remove multicolinearity. Our results show globally well distributed control of teleconnection indices on temperature, precipitation and radiation interannual changes (Fig. S9). The extensive controls also could be explained by inherently strong correlations among temperature, precipitation and radiation (Fig. S4). The results in Fig. S9 indicate that the eight leading teleconnection indices control all three meteorological variables. The recent period from 2001 to 2011 show stronger role of teleconnection indices on the interannual variabilities of temperature and precipitation compared to the longer term roles during 1982–2011.

Climate-induced crop yield forecasting skills of winter time climatic variability

We analyse the interannual relationships between winter time teleconnection indices and national and state level growing season integrated NDVI, the latter as a proxy of crop yield productivity in relation to changes in climatic variables in line with recent developments presented in several studies (Garnett *et al*., 1998; Hsieh *et al*., 1999; Quiring & Blair, 1999; Iizumi *et al*., 2014; Gonsamo & Chen, 2015). We do not use national crop yield inventory as crop management intensity and harvest index (ratio of yield to biomass) have been increasing substantially (e.g., Hay, 1995; Johnson *et al*., 2006; Lorenz *et al*., 2010) since the Green Revolution in the 1960s. Therefore, yield may not directly translate to crop photosynthetic productivity in response to climatic variability. In this study, we use the growing season NDVI as a direct proxy of climate-induced crop yield productivity indicator. We use the detrended teleconnection and NDVI datasets and calculate the slope and *P*-value (two-tailed Student's *t*-test) pixel-by-pixel using ordinary least squares linear regression. Then, we average both slope and *P*-value at country and USA state levels. We only report those countries and USA states for which the averaged *P*-value is <0.05.

The winter teleconnection indices can successfully ($P < 0.05$) predict the growing season NDVI in several countries in Europe and few in Africa, and 16 states in the USA (Table 1, Table 2). NAO and SCA are the most prominent predictors in Europe during the concurrent calendar year. NINO, PNA and WR predict the growing season NDVI of several states in USA six seasons ahead (Table 2). The nature of winter teleconnection indices, and changes in their behaviour, including predictably of rainfall, snowfall, droughts, heat wave or temperature patterns with at least two seasons lead time, are central for agricultural crop yield forecasting. Our findings highlight the strong importance of winter teleconnection indices to global crop production forecasting by providing early warning during unfavourable climate regimes ahead of cropping season to operationally plan potential management options and produce an economically viable yield.

Discussion

Trends in NDVI and interannual covariability with climate

The GIMMS NDVI dataset has been widely used for detecting vegetation growth change (Peng *et al*., 2013; Pinzon & Tucker, 2014; Poulter *et al*., 2014) and extensively used as an indicator of primary productivity of the terrestrial biosphere (Myneni *et al*., 1997; Zhou *et al*., 2001). Our results are in agreement with previous study (Jong *et al*., 2012), which presents detailed analyses of short-term and long-term geographic distributions of trends. Although the precipitation is increasing

in the arid zones of the northern Sahel and the southern Sahara (Fig. 1e), the increased temperature (Fig. 1g) results in enhanced moisture stress through greater water demand which may explain the decline in vegetation greenness on these regions. This is further supported by the strong control of both precipitation and temperature on the interannual changes of vegetation greenness in the arid zones of the northern Sahel and the southern Sahara (Fig. 1f,h).

The global-scale increase in vegetation productivity for 1982–2011 (Fig. 1a) is in a good agreement with earlier modelling and satellite-based studies which were conducted for shorter and earlier time periods after 1980s (Nemani *et al*., 2003; Cao *et al*., 2004; Running *et al*., 2004; De Jong *et al*., 2011; Jong *et al*., 2012). Zhao & Running (2010) reported recent drought-induced decline in global primary productivity for 2000–2009 period. Our results also show, 2000–2009 remain well below the global average of 1982–2011 NDVI except for year 2001 albeit not declining (Fig. S5). Increases in wildfire frequency, and warming induced increases in moisture stress through greater water demands amplified by the decline in northern hemisphere ice extent partly explains the declining greenness in the boreal Canada (Girardin *et al*., 2013). The remaining variance in decline in boreal Canada could be explained by the delayed spring activity and greenup of vegetation due to persistently positive NAO for 20 out of 30 years during the study period. Tropical areas are never limited by temperature alone (Figs 1 and S3) but long-term increases in temperatures in Amazon and Congo forests, possibly coinciding with other growth enhancing global changes and meteorological variables may explain the long-term relationship between temperature and NDVI in these regions (Fig. S1a).

PDO and AMO explain most of the long-term trend in NDVI (Fig. 1a–c). PDO explains many of the climatic variabilities observed globally during the post-1998 hiatus with higher continental temperatures and tropical land precipitation (Trenberth *et al*., 2014b) compared to the 1982–1997. Both PDO and AMO modulate other teleconnection patterns and, by inference, their impact on NDVI trends. Although long-term trends in NDVI are the manifestation of many global processes occurring due to the coupling of externally forced climate change and internal climatic variability, human growth and development has been another major factor in altering vegetation productivity through land cover land use change (LCLUC) (e.g., Wright *et al*., 2012; Jeganathan *et al*., 2014). This is particularly evident in the post-1990s cropland abandonment in Eurasian grain belt, the industrial and agricultural heartland of the former Soviet Union (e.g., Wright *et al*., 2012; de Beurs *et al*., 2015). For example, the long-term increases in temperatures (Fig. 1g), persistent positive phase of NAO and its strong control on vegetation productivity (Fig. 3), and possibly coinciding with cropland abandonment and forest regeneration in some part of Eurasian grain belt may explain the long-term increase in NDVI in the region (Fig. 1a). However, detangling and attributing the NDVI trends to climatic and LCLUC factors are beyond the scope of the current work. It should be noted that all of our subsequent analyses are based on interannual covariability after removing long-term trends, to partially remove the influence of unaccounted factors on NDVI changes.

Our results show that most of the earth's vegetated land surfaces are colimited by the three meteorological variables unlike the results presented in previous studies (Churkina & Running, 1998; Nemani *et al*., 2003; Running *et al*., 2004). Our results differ owing partly to the methodological difference and partly to increased teleconnection patterns controls on interannual changes in meteorological variables (Fig. S9) and eventually on vegetation productivity during 2001–2011 compared to the 1982–1999 period of Nemani *et al.* (2003) study, which was dominated by steep increases in global temperatures. Another source of difference is the modelled potential geographic limits of the three meteorological variables presented in previous studies (Churkina & Running, 1998; Nemani *et al*., 2003; Running *et al*., 2004) are more spatially homogeneous than the actual measured geographic distribution of growth limits presented in this study. While it is easy to imagine the modelled potential limits such as Amazon and Congo vegetations as radiation limited and global arid zones as water limited, heterogeneity in land cover and biome (e.g., difference in Amazon savannah and Amazon forest, arid zones of north Africa, south Africa, Australia and Eurasia) makes the three climatic variables colimit vegetation growth in a complex manner at local scale. Our results show that vegetated areas in northern hemisphere those controlled by temperature (Figs 1d and S3) are highly affected by temperature mediated influence NAO and SCA patterns (Figs 3 and 4).

Vegetation productivity responses to climatic variability

Our results, based on three decades of satellite observations, suggest that teleconnection patterns dominate the interannual variability of continental vegetation productivity, similar to their strong role on terrestrial evaporation patterns (Miralles *et al*., 2013). Winter teleconnections show strong potential in predicting overall vegetation productivity. Winter NAO and SCA alone can predict the central European vegetation productivity during the ensuing growing season (Table 1). Given the recurring drought and devastating

heat-waves (Trnka *et al*., 2014) on European crop production, NAO and SCA appear to be indispensable early warning tools (Gonsamo & Chen, 2015) for farmers to plan management options to minimize yield losses during the growing season summer months.

Unlike a single meteorological variable, teleconnection patterns control heat, moisture and momentum balances through their effects on temperature, precipitation and solar radiation reaching the Earth's surface (Fig. S9), the latter through changes in cloudiness. The water vapour loading due to teleconnections also affects humidity and leaf-to-air vapour pressure deficit within the soil-plant-atmosphere continuum. The recent stronger role of teleconnection indices on the interannual variabilities of temperature and precipitation (Fig. S9) could be explained by relatively eased, possibly saturated, recent anthropogenic forcing on interannual climatic variability compared to those caused by natural ocean-atmosphere variations (Kosaka & Xie, 2013; England *et al*., 2014; Meehl *et al*., 2014). This however remains to be verified.

Our results indicate that teleconnection patters may continue to be an important aspect of future regional terrestrial ecosystem productivity given that the anthropogenic global changes in climate is expected to ease several critical climatic constraints to plant growth (Zhao & Running, 2010). New evidence is emerging that suggests external forcing precursors, including aerosols and greenhouse gas forcing, may intensify internal climatic variations (Knudsen *et al*., 2014). However, challenges remain in separating the long-term relative roles of natural climatic variation and anthropogenic forcing on vegetation productivity, and Earth system models do not always capture the role of internal variability.

The lack of significant trends in regionally averaged CCSM4 mean NPP values (Fig. S8) shows that CCSM4 simulations do not capture the productivity responses to recent growth enhancing changes in meteorological variables. The CCSM4 simulations in this study were forced using the measured historic meteorological variables. Although the unforced CCSM4 simulations resulted in comparable carbon flux variability to the observations at the Harvard Forest eddy covariance flux tower site (Lombardozzi *et al*., 2014), several Earth system models are not developed to capture the global ocean-atmosphere system variations. Given the ubiquitous control of teleconnections on vegetation productivity (Figs 2 and 3) through their impact on regional meteorological variables (Fig. 4), representation of internal climatic variations in CCSM4 can be improved by using the observed vegetation response patterns to guide further model development.

Acknowledgements

We thank the Climatic Research Unit, National Aeronautics and Space Administration Clouds and Earth's Radiant Energy System, National Oceanic and Atmospheric Administration National Weather Service and National Climatic Data Center, Compton J. Tucker, and the Global Inventory Modelling and Mapping Studies team for making their data available. We thank Kevin E Trenberth for valuable discussions throughout the preparation of the manuscript. We would like to thank the four anonymous referees for the helpful comments.

References

Barnston AG, Livezey RE (1987) Classification, seasonality and persistence of low-frequency atmospheric circulation patterns. *Monthly Weather Review*, **115**, 1083–1126.

Behrenfeld MJ, Randerson JT, Mcclain CR *et al*. (2001) Biospheric primary production during an ENSO transition. *Science*, **291**, 2594–2597.

de Beurs KM, Henebry GM, Owsley BC, Sokolik I (2015) Using multiple remote sensing perspectives to identify and attribute land surface dynamics in Central Asia 2001–2013. *Remote Sensing of Environment*, **170**, 48–61.

Cao M, Prince SD, Small J, Goetz SJ (2004) Remotely sensed interannual variations and trends in terrestrial net primary productivity 1981–2000. *Ecosystems*, **7**, 233–242.

Churkina G, Running SW (1998) Contrasting climatic controls on the estimated productivity of global terrestrial biomes. *Ecosystems*, **1**, 206–215.

Dai A, Qian T, Trenberth KE, Milliman JD (2009) Changes in continental freshwater discharge from 1948 to 2004. *Journal of Climate*, **22**, 2773–2792.

De Jong R, De Bruin S, De Wit A, Schaepman ME, Dent DL (2011) Analysis of monotonic greening and browning trends from global NDVI time-series. *Remote Sensing of Environment*, **115**, 692–702.

Defries R, Townshend J (1994) NDVI-derived land cover classification at a global scale. *International Journal of Remote Sensing*, **15**, 3567–3586.

England MH, Mcgregor S, Spence P *et al*. (2014) Recent intensification of wind-driven circulation in the Pacific and the ongoing warming hiatus. *Nature Climate Change*, **4**, 222–227.

Fu QA (1996) An accurate parameterization of the solar radiative properties of cirrus clouds for climate models. *Journal of Climate*, **9**, 2058–2082.

Fu Q, Liou KN (1992) On the correlated k-distribution method for radiative-transfer in nonhomogeneous atmospheres. *Journal of the Atmospheric Sciences*, **49**, 2139–2156.

Fu Q, Liou KN (1993) Parameterization of the radiative properties of cirrus clouds. *Journal of the Atmospheric Sciences*, **50**, 2008–2025.

Fu Q, Yang P, Sun WB (1998) An accurate parameterization of the infrared radiative properties of cirrus clouds for climate models. *Journal of Climate*, **11**, 2223–2237.

Garnett E, Khandekar M, Babb J (1998) On the utility of ENSO and PNA indices for long-lead forecasting of summer weather over the crop-growing region of the Canadian Prairies. *Theoretical and Applied Climatology*, **60**, 37–45.

Girardin MP, Guo XJ, De Jong R, Kinnard C, Bernier P, Raulier F (2013) Unusual forest growth decline in boreal North America covaries with the retreat of Arctic sea ice. *Global Change Biology*, **20**, 851–866.

Gong D-Y, Shi P-J (2003) Northern hemispheric NDVI variations associated with large-scale climate indices in spring. *International Journal of Remote Sensing*, **24**, 2559–2566.

Gonsamo A, Chen JM (2015) Winter teleconnections can predict the ensuing summer European crop productivity. *Proceedings of the National Academy of Sciences of USA*, **112**, E2265–E2266.

Gonsamo A, Chen JM, D'Odorico P (2015) Underestimated role of East Atlantic-West Russia pattern on Amazon vegetation productivity. *Proceedings of the National Academy of Sciences of USA*, **112**, E1054–E1055.

Harris I, Jones PD, Osborn TJ, Lister DH (2014) Updated high-resolution grids of monthly climatic observations - the CRU TS3.10 Dataset. *International Journal of Climatology*, **34**, 623–642.

Hay RKM (1995) Harvest index - a review of its use in plant-breeding and crop physiology. *Annals of Applied Biology*, **126**, 197–216.

Hird JN, Mcdermid GJ (2009) Noise reduction of NDVI time series: an empirical comparison of selected techniques. *Remote Sensing of Environment*, **113**, 248–258.

Hsieh WW, Tang B, Garnett ER (1999) Teleconnections between Pacific sea surface temperatures and Canadian prairie wheat yield. *Agricultural and Forest Meteorology*, **96**, 209–217.

Hurrell JW, Deser C (2010) North Atlantic climate variability: the role of the North Atlantic Oscillation. *Journal of Marine Systems*, **79**, 231–244.

Iizumi T, Luo J-J, Challinor AJ *et al.* (2014) Impacts of El Niño Southern Oscillation on the global yields of major crops. *Nature Communication*, **5**, 3712.

IPCC (2007) *IPCC Fourth Assessment Report: Climate Change 2007 (AR4)*. Cambridge University Press, Cambridge, UK and New York, NY, USA.

Jeganathan C, Dash J, Atkinson PM (2014) Remotely sensed trends in the phenology of northern high latitude terrestrial vegetation, controlling for land cover change and vegetation type. *Remote Sensing of Environment*, **143**, 154–170.

Johnson JF, Allmaras R, Reicosky D (2006) Estimating source carbon from crop residues, roots and rhizodeposits using the national grain-yield database. *Agronomy Journal*, **98**, 622–636.

Jong R, Verbesselt J, Schaepman ME, Bruin S (2012) Trend changes in global greening and browning: contribution of short-term trends to longer-term change. *Global Change Biology*, **18**, 642–655.

Kaplan A, Cane MA, Kushnir Y, Clement AC, Blumenthal MB, Rajagopalan B (1998) Analyses of global sea surface temperature 1856-1991. *Journal of Geophysical Research-Oceans*, **103**, 18567–18589.

Kato S, Loeb NG, Rose FG *et al.* (2013) Surface Irradiances Consistent with CERES-derived top-of-atmosphere shortwave and longwave irradiances. *Journal of Climate*, **26**, 2719–2740.

Knudsen MF, Jacobsen BH, Seidenkrantz M-S, Olsen J (2014) Evidence for external forcing of the Atlantic Multidecadal Oscillation since termination of the Little Ice Age. *Nature Communication*, **5**, 3323.

Kosaka Y, Xie S-P (2013) Recent global-warming hiatus tied to equatorial Pacific surface cooling. *Nature*, **501**, 403–407.

Lau N-C, Nath MJ (1994) A modeling study of the relative roles of tropical and extratropical SST anomalies in the variability of the global atmosphere-ocean system. *Journal of Climate*, **7**, 1184–1207.

Lombardozzi D, Bonan GB, Nychka DW (2014) The emerging anthropogenic signal in land-atmosphere carbon-cycle coupling. *Nature Climate Change*, **4**, 796–800.

Lorenz A, Gustafson T, Coors J, Leon ND (2010) Breeding maize for a bioeconomy: a literature survey examining harvest index and stover yield and their relationship to grain yield. *Crop Science*, **50**, 1–12.

Macias-Fauria M, Forbes BC, Zetterberg P, Kumpula T (2012) Eurasian Arctic greening reveals teleconnections and the potential for structurally novel ecosystems. *Nature Climate Change*, **2**, 613–618.

Markon CJ, Fleming MD, Binnian EF (1995) Characteristics of vegetation phenology over the Alaskan landscape using AVHRR time-series data. *Polar Record*, **31**, 179–190.

Meehl GA, Teng H, Arblaster JM (2014) Climate model simulations of the observed early-2000s hiatus of global warming. *Nature Climate Change*, **4**, 898–902.

Miralles DG, Van Den Berg MJ, Gash JH *et al.* (2013) El Niño–La Niña cycle and recent trends in continental evaporation. *Nature Climate Change*, **4**, 122–126.

Myneni RB, Keeling CD, Tucker CJ, Asrar G, Nemani RR (1997) Increased plant growth in the northern high latitudes from 1981 to 1991. *Nature*, **386**, 698–702.

Nemani RR, Keeling CD, Hashimoto H *et al.* (2003) Climate-driven increases in global terrestrial net primary production from 1982 to 1999. *Science*, **300**, 1560–1563.

Patra PK, Maksyutov S, Nakazawa T (2005) Analysis of atmospheric CO2 growth rates at Mauna Loa using CO2 fluxes derived from an inverse model. *Tellus Series B*, **57**, 357–365.

Peng S, Piao S, Ciais P *et al.* (2013) Asymmetric effects of daytime and night-time warming on Northern Hemisphere vegetation. *Nature*, **501**, 88–92.

Pinzon J, Tucker C (2014) A Non-Stationary 1981–2012 AVHRR NDVI3g Time Series. *Remote Sensing*, **6**, 6929–6960.

Poulter B, Frank D, Ciais P *et al.* (2014) Contribution of semi-arid ecosystems to interannual variability of the global carbon cycle. *Nature*, **509**, 600–603.

Quadrelli R, Wallace JM (2004) A simplified linear framework for interpreting patterns of Northern Hemisphere wintertime climate variability. *Journal of Climate*, **17**, 3728–3744.

Quiring S, Blair D (1999) *The Utility of Global Teleconnection Indices for Long-Range Crop Forecasting on the Canadian Prairies*. University of Winnipeg, Winnipeg, Manitoba, Canada.

Running SW, Nemani RR, Heinsch FA, Zhao M, Reeves M, Hashimoto H (2004) A continuous satellite-derived measure of global terrestrial primary production. *BioScience*, **54**, 547–560.

Sheng J (1999) Correlation between the Pacific/North American pattern and the eastward propagation of sea surface temperature anomalies in the North Pacific. *Journal of Geophysical Research: Atmospheres*, **104**, 30885–30895.

Smith TM, Reynolds RW, Peterson TC, Lawrimore J (2008) Improvements to NOAA's historical merged land-ocean surface temperature analysis (1880-2006). *Journal of Climate*, **21**, 2283–2296.

Trenberth KE, Smith L (2005) The mass of the atmosphere: a constraint on global analyses. *Journal of Climate*, **18**, 864–875.

Trenberth KE, Dai A, Van Der Schrier G, Jones PD, Barichivich J, Briffa KR, Sheffield J (2014a) Global warming and changes in drought. *Nature Climate Change*, **4**, 17–22.

Trenberth KE, Fasullo JT, Branstator G, Phillips AS (2014b) Seasonal aspects of the recent pause in surface warming. *Nature Climate Change*, **4**, 911–916.

Trnka M, Rotter RP, Ruiz-Ramos M, Kersebaum KC, Olesen JE, Zalud Z, Semenov MA (2014) Adverse weather conditions for European wheat production will become more frequent with climate change. *Nature Climate Change*, **4**, 637–643.

Wallace JM, Gutzler DS (1981) Teleconnections in the geopotential height field during the Northern Hemisphere winter. *Monthly Weather Review*, **109**, 784–812.

Woodward F, Lomas M, Quaife T (2008) Global responses of terrestrial productivity to contemporary climatic oscillations. *Philosophical Transactions of the Royal Society B: Biological Sciences*, **363**, 2779–2785.

Wright CK, de Beurs KM, Henebry GM (2012) Combined analysis of land cover change and NDVI trends in the Northern Eurasian grain belt. *Frontiers of Earth Science*, **6**, 177–187.

Zhao M, Running SW (2010) Drought-induced reduction in global terrestrial net primary production from 2000 through 2009. *Science*, **329**, 940–943.

Zhou LM, Tucker CJ, Kaufmann RK, Slayback D, Shabanov NV, Myneni RB (2001) Variations in northern vegetation activity inferred from satellite data of vegetation index during 1981 to 1999. *Journal of Geophysical Research-Atmospheres*, **106**, 20069–20083.

Supporting Information

Additional Supporting Information may be found in the online version of this article:

Table S1. Correlation matrix of all detrended teleconnection indices.
Table S2. Variances (%) explained by each teleconnection index at various principal components (PCAs).
Figure S1. NDVI responses to long-term variabilities in annual growing season temperature and precipitation for 1982–2011.
Figure S2. Impacts of eight leading teleconnection patterns on global annual growing season NDVI anomaly during teleconnection phase years at different spatial resolutions.
Figure S3. Discrete map of the geographic distribution of temperature (T), precipitation (P) and solar radiation (R) controls on vegetation productivity for 2001 2011.
Figure S4. Relationships among annual growing season temperature, precipitation and radiation for 2001–2011.
Figure S5. Detrended global and continental mean annual growing season sums of NDVI and teleconnection index anomalies.
Figure S6. Global and continental NDVI annual growing season sum anomaly responses to negative and positive teleconnection index phases during and one year after each phase of teleconnection index years.
Figure S7. Impacts of eight leading teleconnection patterns on global growing season NDVI and NPP anomalies during and the ensuing teleconnection phase years.
Figure S8. Trends of global and continental mean annual growing season sums of NDVI and mean annual NPP from the Community Climate System Model version 4 seven-member ensemble gridded values.
Figure S9. Geographic distributions of limits of eight leading teleconnections on temperature (T), precipitation (P) and radiation (R) derived from measured teleconnection and climatic data.